Monoenergetic Proton Radiography Measurements of Implosion Dynamics in Direct-Drive Inertial Confinement Fusion

The goal of inertial confinement fusion (ICF) is ignition and high gain,[1–3] which require that a cryogenic deuterium–tritium (DT) spherical capsule be symmetrically imploded. This implosion results in a small mass of low-density, hot fuel at the center, surrounded by a larger mass of high-density, low-temperature fuel.[2,3] Shock coalescence ignites the hot spot, and a self-sustaining burn wave subsequently propagates into the main fuel region. In the direct-drive approach to ICF, such an implosion occurs in response to a large number of high-power individual laser beams illuminating the surface of a capsule. Understanding and controlling implosion dynamics are essential to ensure the success of the entire implosion process.[1–3]

Implosion dynamics have been studied experimentally with a number of diagnostics, including x-ray imaging,[2–5] fusion-product spectrometry,[6] and fusion-product imaging,[7,8] but none of these provide a complete picture of the time evolution of mass assembly and self-generated electric (E) and magnetic (B) fields.

This article presents new nuclear observations of implosion dynamics for direct-drive spherical capsules on the OMEGA Laser System,[9] using a novel method of monoenergetic proton radiography.[10,11] The combination of characteristics in our approach allows us to, first, probe distributions of self-generated E + B fields; second, determine ρR by measuring the energy loss of backlighting protons; and third, sample all the implosion phases from acceleration, through coasting and deceleration, to final stagnation, to provide a more-comprehensive picture of ICF spherical implosions. The result is the first use of proton radiography to study ICF implosion dynamics. We note that earlier work by Mackinnon *et al.*[12] successfully demonstrated the feasibility of imaging implosions with protons (produced, in his case, by laser–plasma interactions), backlighting plastic (CH) capsules that were imploded by six 1-μm-wavelength laser beams.[13]

The experiment is illustrated schematically in Fig. 114.31. A CH capsule—the imaged subject—had an 860-μm initial diameter, a 20-μm-thick shell, and a 15-atm H_2 gas fill. It was imploded through direct drive with 40 beams of frequency-tripled (0.35 μm) UV laser light. The laser pulse was square, with a 1-ns duration and a total energy of ~16 kJ. The individual laser beams were smoothed using a single-color-cycle, 1-THz, two-dimensional (2-D) smoothing by spectral dispersion (SSD), and polarization smoothing (PS).[14,15] Implosions were backlit with monoenergetic protons (14.7 MeV) generated from D^3He-filled, exploding-pusher implosions driven by 19 OMEGA laser beams (details of this technology have been reported elsewhere[10,11]). The duration of the backlighting was ~130 ps, and the relative timing of backlighter and subject implosions was adjusted in each experiment so the proton radiograph would reflect the condition of the subject capsule at a desired time during its implosion. The effective FWHM of the backlighter was ≈40 μm (Ref. 10)—the primary limit on the intrinsic spatial resolution of the imaging system. In images of imploded capsules, spatial resolution was degraded somewhat by scattering of the imaging protons as they passed through the capsules.[16,17]

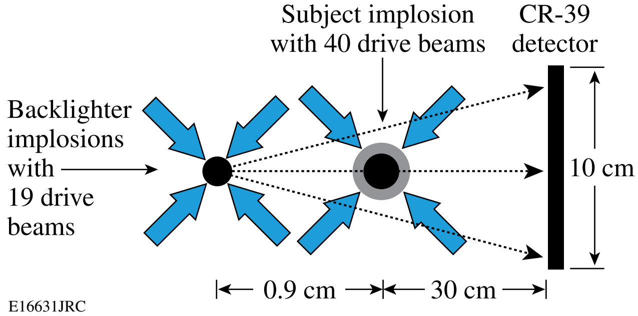

Figure 114.31
Experimental setup, with proton backlighter, subject implosion, CR-39 imaging detectors and laser beams. The field of view at the subject is ~3 mm.

Figure 114.32 shows a series of proton radiographs that cover a complete ICF implosion process from beginning through peak compression. Each individual image contains both spatial and energy information because the CR-39 detector records the position and energy of every individual proton. Such images can therefore be displayed to show either proton fluence versus position [Fig. 114.32(a)] or proton mean energy versus position [Fig. 114.32(b)], providing important information about field distributions and capsule compression.

A striking feature of Fig. 114.32(a) is that a central peak occurs in the fluence images during the early stages of implosion (t = 0.8 to 1.4 ns), while a fluence dip occurs at the centers at later times (t = 1.6 to 2.1 ns).[19] This indicates that trajectories of imaging protons were deflected by radial E fields in the capsule. (Proton trajectories are also altered by scattering in the capsule shell, but this process cannot account for the observed fluence peaks and dips.[20]) At early times the field must have been centrally directed in order to focus the protons passing within the capsule shell toward the center of the imaging detector. To account for the rapid change from a central fluence peak to a central fluence dip at ~1.5 ns, the radial field must have either reversed direction or suddenly become at least three times larger at that time (as shown by Monte Carlo simulations), in which case all protons would strike the detector outside the shadow of the capsule.

An E-field source that is consistent with the data is the gradient of plasma electron pressure $\left(E \approx -\nabla p_e / e n_e\right)$.[21,22] Other possible sources do not fit as naturally with the data.[23] The pressure gradient has the correct sign at early times, and it reverses direction at about the correct time. This is illustrated in the electron pressure and density profiles at 0.8 ns and 1.9 ns, calculated by the *LILAC* hydro simulation program[24] and shown in Fig. 114.33. Using calculated ∇p_e and n_e at different times, we estimate the resultant E-field magnitude in the range ~ -10^9 to ~10^8 V/m, as shown in Fig. 114.34. Figure 114.34 also shows experimental field values deduced from the data of Fig. 114.32(a).[25] The predictions match the data in three crucial ways: the field strength and sign before the reversal (~ -10^9 V/m, directed inward), the time of the field reversal (~1.5 ns), and the field strength after the reversal (~10^8 V/m directed outward). This match leads to a high level of confidence that ∇p_e is the source of the observed phenomena. Note that the detailed structures of the fluence images in Fig. 114.32(a) are also modified, in ways that do not affect our conclusions, by the in-flight movement of the shell (V_{imp} ~ -2.5×10^7 cm/s), which is ~30 μm during the backlighter nuclear burn time (~130 ps).

Quantitative information about capsule sizes and ρR's at different times is extracted from the lineouts through the centers of each of the individual images in Fig. 114.32(b); the mean

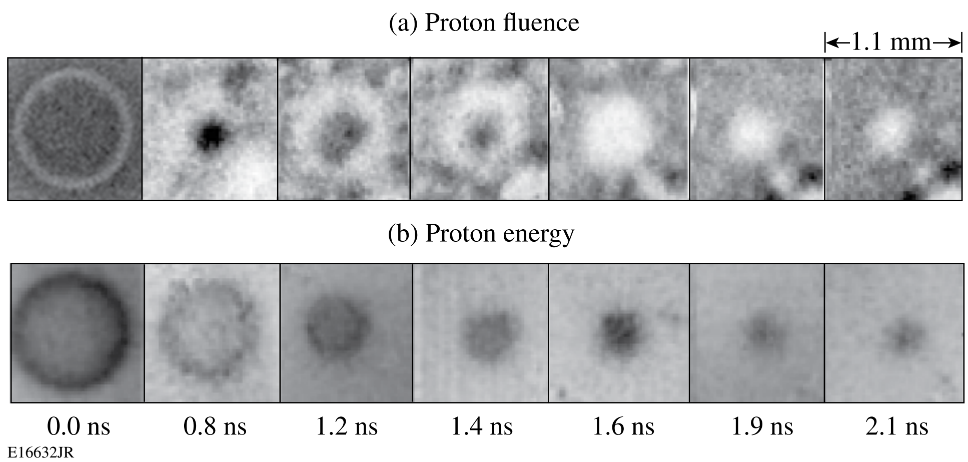

Figure 114.32
Proton radiographs of imploding capsules at different times. Images in (a) show proton fluence (within each image, darker means higher fluence), while images in (b) show proton energy (within each image, darker means more proton energy loss and more matter traversed). The gray-scale mapping for image display is different in each image. Note that the capsule-mounting stalk appears in the lower right corner of each fluence image. Note also that the field of view of these images is only part of the total indicated in Fig. 114.31; the area outside this region is the subject of another study of external fields.[18]

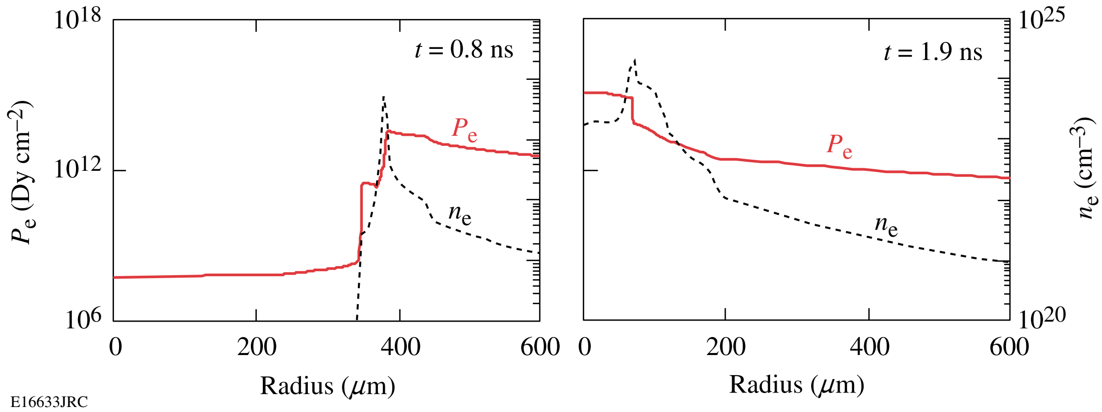

Figure 114.33
Profiles of electron pressure (solid lines) and density (dashed lines) at 0.8 ns and 1.9 ns, calculated by *LILAC*.

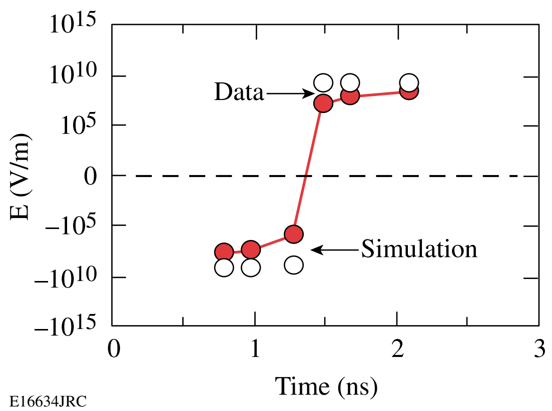

Figure 114.34
Radial E fields estimated from experimental measurements (open circles) and from *LILAC* simulations (solid circles) versus implosions times. The differences between simulation and data may result from effects of proton scattering.

width provides the averaged capsule size (≈2R), while the mean height indicates the total ρL (≈2 × ρR). The measurements are compared with *LILAC* simulations in Figs. 114.35(a) and 114.35(b), respectively. The simulations come reasonably close to matching the observed evolution of capsule convergence and ρR during the acceleration and coasting phases (~0 to 1.6 ns), but they predict somewhat smaller values of radius, and larger values of ρR, than measured at the times of nuclear burn (~1.9 ns) and peak compression (~2.1 ns). Overall, this indicates that the implosions had approximately 1-D performance, with little impact from hydrodynamic instabilities, before deceleration. It has been suggested that performance approaches 1-D because of full single-beam smoothing, which significantly improves the shell integrity during the acceleration phase, and because thickening of the shell during subsequent coasting further enhances shell integrity.[15] The apparent degradation of capsule performance at later times relative to the 1-D simulation could be largely a consequence of fuel–shell mixing and implosion asymmetry.[2,3]

It is worthwhile to compare these measured ρR values with a value obtained using a completely different method during an equivalent implosion. The open black data point in Fig. 114.35(b) was obtained by using proton spectrometry to determine the energy of self-emitted D^{3}He protons;[26] the downshift in the energy of these protons implies a ρR at bang time of ~25 mg/cm^2. This is slightly higher than the measurement made here but statistically consistent with it given the measurement uncertainties. On the other hand, the spectrometry-implied value is closer to the 1-D value, which raises the possibility that the radiography-implied value loses accuracy when the capsule becomes sufficiently compressed that images are seriously affected by proton scatter. This is currently being investigated, and we plan to develop a more accurate technique for deconvolving the effects of scatter in our analyses.

Finally, the residual mass during the implosion process can be estimated in terms of the measured R [Fig. 114.35(a)] and measured ρR [Fig. 114.35(b)]: $m/m_0 \approx C_r^{-2}\,\rho R(t)/\rho R(0)$, where $C_r \equiv R(0)/R(t)$ is the target convergence ratio. This indicates that ~30%–40% of the shell has been ablated by bang time. Although the mass estimates have large uncertainties due to those associated with both R and ρR measurements, they are helpful for illustrating the dynamics of mass ablation during implosions.

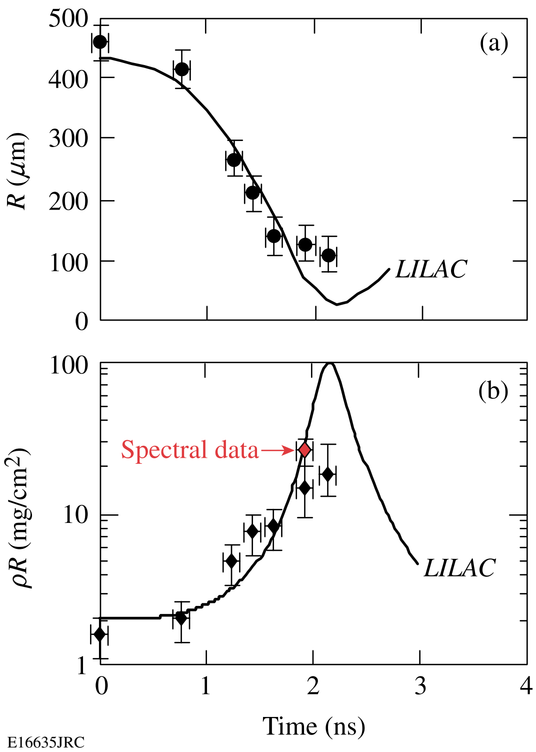

Figure 114.35
Measured capsule radii [(a) solid circles] and ρR [(b) solid diamonds] compared with *LILAC* 1-D simulations (solid lines). Horizontal error bars represent uncertainties in backlighter burn time. One data point [open diamond in (b)] represents the ρR of a comparable implosion of a D^3He-filled capsule at bang time, measured by several proton spectrometers in different directions; this completely different type of measurement is statistically consistent with the data derived here from radiography images.

In summary, new observations and measurements of direct-drive spherical implosions have been made with time-gated, monoenergetic proton radiography. Quantitative information inferred from proton images characterizes the spatial structure and temporal evolution of an imploding capsule, dynamically displaying a more-comprehensive picture of direct-drive ICF spherical implosions. The observations have also shown the first experimental evidence of radial E fields inside the imploding capsules, as well as their reversal in direction and their probable connection with plasma pressure gradients.

ACKNOWLEDGMENT

The work described here was performed at the LLE National Laser Users' Facility (NLUF) and was supported in part by U.S. DOE (Grant No. DE-FG03-03SF22691), LLE (subcontract Grant No. 412160-001G), LLNL (subcontract Grant No. B504974), the Fusion Science Center for Extreme States of Matter and Fast Ignition Physics at the University of Rochester, and GA under DOE (DE-AC52-06NA27279).

REFERENCES

1. J. Nuckolls *et al*., Nature **239**, 139 (1972).
2. J. D. Lindl, *Inertial Confinement Fusion: The Quest for Ignition and Energy Gain Using Indirect Drive* (Springer-Verlag, New York, 1998).
3. S. Atzeni and J. Meyer-ter-Vehn, *The Physics of Inertial Fusion: Beam Plasma Interaction, Hydrodynamics, Hot Dense Matter*, International Series of Monographs on Physics (Clarendon Press, Oxford, 2004).
4. F. J. Marshall, J. A. Delettrez, R. Epstein, R. Forties, R. L. Keck, J. H. Kelly, P. W. McKenty, S. P. Regan, and L. J. Waxer, Phys. Plasmas **11**, 251 (2004).
5. R. S. Craxton, F. J. Marshall, M. J. Bonino, R. Epstein, P. W. McKenty, S. Skupsky, J. A. Delettrez, I. V. Igumenshchev, D. W. Jacobs-Perkins, J. P. Knauer, J. A. Marozas, P. B. Radha, and W. Seka, Phys. Plasmas **12**, 056304 (2005).
6. F. H. Séguin, J. A. Frenje, C. K. Li, D. G. Hicks, S. Kurebayashi, J. R. Rygg, B.-E. Schwartz, R. D. Petrasso, S. Roberts, J. M. Soures, D. D. Meyerhofer, T. C. Sangster, J. P. Knauer, C. Sorce, V. Yu. Glebov, C. Stoeckl, T. W. Phillips, R. J. Leeper, K. Fletcher, and S. Padalino, Rev. Sci. Instrum. **74**, 975 (2003).
7. L. Disdier, A. Rouyer, I. Lantuéjoul, O. Landoas, J. L. Bourgade, T. C. Sangster, V. Yu. Glebov, and R. A. Lerche, Phys. Plasmas **13**, 056317 (2006).
8. F. H. Séguin, J. L. DeCiantis, J. A. Frenje, S. Kurebayashi, C. K. Li, J. R. Rygg, C. Chen, V. Berube, B. E. Schwartz, R. D. Petrasso, V. A. Smalyuk, F. J. Marshall, J. P. Knauer, J. A. Delettrez, P. W. McKenty, D. D. Meyerhofer, S. Roberts, T. C. Sangster, K. Mikaelian, and H. S. Park, Rev. Sci. Instrum. **75**, 3520 (2004).
9. J. M. Soures, R. L. McCrory, C. P. Verdon, A. Babushkin, R. E. Bahr, T. R. Boehly, R. Boni, D. K. Bradley, D. L. Brown, R. S. Craxton, J. A. Delettrez, W. R. Donaldson, R. Epstein, P. A. Jaanimagi, S. D. Jacobs, K. Kearney, R. L. Keck, J. H. Kelly, T. J. Kessler, R. L. Kremens, J. P. Knauer, S. A. Kumpan, S. A. Letzring, D. J. Lonobile, S. J. Loucks, L. D. Lund, F. J. Marshall, P. W. McKenty, D. D. Meyerhofer, S. F. B. Morse, A. Okishev, S. Papernov, G. Pien, W. Seka, R. Short, M. J. Shoup III, M. Skeldon, S. Skupsky, A. W. Schmid, D. J. Smith, S. Swales, M. Wittman, and B. Yaakobi, Phys. Plasmas **3**, 2108 (1996).
10. C. K. Li, F. H. Séguin, J. A. Frenje, J. R. Rygg, R. D. Petrasso, R. P. J. Town, P. A. Amendt, S. P. Hatchett, O. L. Landen, A. J. Mackinnon, P. K. Patel, V. Smalyuk, J. P. Knauer, T. C. Sangster, and C. Stoeckl, Rev. Sci. Instrum. **77**, 10E725 (2006).
11. C. K. Li, F. H. Séguin, J. A. Frenje, J. R. Rygg, R. D. Petrasso, R. P. J. Town, P. A. Amendt, S. P. Hatchett, O. L. Landen, A. J. Mackinnon,

P. K. Patel, V. A. Smalyuk, T. C. Sangster, and J. P. Knauer, Phys. Rev. Lett. **97**, 135003 (2006).

12. A. J. Mackinnon *et al*., Phys. Rev. Lett. **97**, 045001 (2006).

13. In Ref. 12, Mackinnon reported no fields surrounding the capsule, in contrast to the observations shown here, and this is not presently understood. There are, however, significant differences in the implosion conditions: for example, Mackinnon *et al*. used six beams at 1 μm to irradiate a 250-μm-radius capsule. Herein we used 36 beams at 1/3 μm to irradiate 430-μm-radius capsules. In addition, there are differences in their proton backlighter, such as the fact that the proton spectrum is broadband, a circumstance that will lead to some additional blurring and washout of field structures.

14. S. Skupsky and R. S. Craxton, Phys. Plasmas **6**, 2157 (1999).

15. D. D. Meyerhofer, J. A. Delettrez, R. Epstein, V. Yu. Glebov, V. N. Goncharov, R. L. Keck, R. L. McCrory, P. W. McKenty, F. J. Marshall, P. B. Radha, S. P. Regan, S. Roberts, W. Seka, S. Skupsky, V. A. Smalyuk, C. Sorce, C. Stoeckl, J. M. Soures, R. P. J. Town, B. Yaakobi, J. D. Zuegel, J. Frenje, C. K. Li, R. D. Petrasso, D. G. Hicks, F. H. Séguin, K. Fletcher, S. Padalino, C. Freeman, N. Izumi, R. Lerche, T. W. Phillips, and T. C. Sangster, Phys. Plasmas **8**, 2251 (2001).

16. V. L. Highland, Nucl. Instrum. Methods **129**, 497 (1975).

17. A simple analytic model[16] can be used to estimate the characteristic scattering angle in radians for protons passing through a plasma with areal density ρL. It is $\langle\theta_{sc}\rangle = z(15\,\mathrm{MeV}/p\beta c)(\rho L/\rho L_{rad})^{1/2}$, where z = 1 for protons, $p\beta c$ = 30 MeV for 15-MeV protons, and ρL_{rad} = 4.34×10^4 mg/cm^2 for carbon. For example, if $\rho L \approx 20$ mg/cm^2, then $\langle\theta_{sc}\rangle \sim 0.6°$.

18. F. H. Séguin, C. K. Li, J. R. Rygg, J. A. Frenje, R. D. Petrasso, R. Betti, O. V. Gotchev, J. P. Knauer, F. J. Marshall, D. D. Meyerhofer, and V. A. Smalyuk, "Monoenergetic Proton Radiography Observations of E and B Field Evolution Outside Imploding, Direct-Drive ICF Capsules," in preparation.

19. It has been confirmed by Monte Carlo simulations of the imaging system that, for a given amount of deflection, the character of focusing or defocusing in the image is relatively insensitive to the specific distance of the detector position.

20. There are two reasons why scatter cannot account for the observed features: First, simulations show that the Coulomb scattering angles are not large enough to deflect protons to the image center at the earlier times. Second, scatter could not account for the level of fluence reduction seen in the center region at later implosion times. Monte Carlo simulations indicate that proton scattering at later times reduces the central proton fluence in radiographs by ~30% relative to values outside the capsule. The reductions in the actual images [Fig. 114.32(b)] are ~90%, indicating that scattering is not the dominant mechanism behind the observed central fluence deficit.

21. L. Spitzer, *Physics of Fully Ionized Gases*, 2nd rev. ed., Interscience Tracts on Physics and Astronomy (Interscience, New York, 1962).

22. S. I. Braginskii, in *Reviews of Plasma Physics*, edited by Acad. M. A. Leontovich (Consultants Bureau, New York, 1965).

23. For example, the charge separation around the convergent shock front due to the imbalance of ion mean free paths between the shocked and unshocked plasmas. This contribution can be ruled out as the dominant source because it will neither reverse direction nor suddenly increase as the data require. (We have ignored contributions from the outgoing shock front at later times due to its relatively weaker strength.)

24. J. Delettrez, R. Epstein, M. C. Richardson, P. A. Jaanimagi, and B. L. Henke, Phys. Rev. A **36**, 3926 (1987).

25. The electric field E was derived from the images by using E ~ $2\zeta\varepsilon_p\,(A + a)\,(eAaL)^{-1}$, where ε_p = 15 MeV is the proton energy; e is electron charge; a = 0.9 cm and A = 30.9 cm are distances from backlighter to implosion and from backlighter to detector, respectively; $|\zeta| \sim (0.5–1) \times R$ is the apparent displacement of protons in the subject plane due to the effects of E on the proton trajectories; and $L \sim (0.5–2) \times R$ is the proton pathlength.

26. C. K. Li, D. G. Hicks, F. H. Séguin, J. A. Frenje, R. D. Petrasso, J. M. Soures, P. B. Radha, V. Yu. Glebov, C. Stoeckl, D. R. Harding, J. P. Knauer, R. L. Kremens, F. J. Marshall, D. D. Meyerhofer, S. Skupsky, S. Roberts, C. Sorce, T. C. Sangster, T. W. Phillips, M. D. Cable, and R. J. Leeper, Phys. Plasmas **7**, 2578 (2000).